

1995119511

N95-25931

3

44644

P. 5

APPENDIX 8

**Cosmic Ray Particles with Different LET Values
Under Various Thicknesses of Shielding
In Low Altitude Orbits: Calculations
and Cosmos-2044 Measurements**

by

**A.M. Marennny, R.A. Nymmik, A.A. Suslov, E.V. Benton,
A.L. Frank and E.R. Benton**



COSMIC RAY PARTICLES WITH DIFFERENT LET VALUES UNDER VARIOUS THICKNESSES OF SHIELDING IN LOW ALTITUDE ORBITS: CALCULATIONS AND COSMOS-2044 MEASUREMENTS

A. M. MARENENY,* R. A. NYMMIK,† A. A. SUSLOV,† E. V. BENTON,‡ A. L. FRANK‡
and E. R. BENTON‡

*Research Center for Spacecraft Radiation Safety, Moscow 123182, U.S.S.R.; †Institute of Nuclear
Physics, Moscow State University, Moscow 119989, U.S.S.R.; ‡University of San Francisco,
San Francisco, CA 94117, U.S.A.

(Received 24 June 1991; in revised form 9 July 1991)

Abstract—Fluxes of cosmic ray particles with different LET values were measured on board the Cosmos-2044 biosatellite under various thicknesses of shielding by stacks of CR-39 and nitrocellulose plastic nuclear track detectors (mounted outside the satellite). The component composition of the particles detected under shieldings of 0.1–2.5 g cm⁻² is verified by comparing experimental data with the results of model simulations of the fluxes of galactic cosmic ray particles and of radiation belt protons.

1. INTRODUCTION

THE RADIATION fields in the Earth's vicinity are generated by the particles which are commonly grouped, according to some criteria (mainly their origin, composition and energy) into certain components, namely, galactic and solar cosmic rays (GCR and SCR), radiation belt (RB) particles and anomalous fluxes (AF). To date, numerous experiments have been carried out on board Soviet and U.S. spacecraft, yielding copious data on the fluxes and spectra of protons and heavy ions in the Earth's vicinity (see, for example, Benton and Parnell, 1988; Marennny *et al.*, 1987). Almost all of the data have been obtained using solid-state nuclear track detectors (SSNTD) (Marennny, 1987) which are notable for their essential characteristic of a detection threshold expressed by the smallest LET value at which detection is possible.

In the present work, an attempt is made to analyze the components of SSNTD-detected particle fluxes under various thicknesses of shielding. The experimental data are supplemented with simulations calculated by models of the radiation environment. Only GCR and RB particles are included because other heavy cosmic ray components did not penetrate to greater shielding thicknesses than 0.05 g cm⁻² during the Cosmos-2044 flight.

2. EXPERIMENT

The Cosmos-2044 mission lasted for 13.8 days from 15 to 29 September 1989. The biosatellite orbit

was elliptical, with a perigee and apogee of 216 and 294 km, respectively, and an inclination of 82.3°. Four flat, lidded containers holding a variety of dosimetric equipment were mounted outside the satellite.

The experimental results presented here were obtained by processing three SSNTD stacks, one at IBMP (Moscow) and two at USF (San Francisco). The IBMP stack of 90 × 50 × 16 mm dimensions contained 20 Soviet-made KNC-type nitrocellulose detectors of 800 μm thickness each. The detectors were etched in a 6N NaOH solution for 5 h at 50 °C. The tracks were scanned with a stereo-microscope at 80 × magnification. The penetrating (a cylinder or two cones) or single-cone (of at least 100 μm length) tracks were selected by counting, and correspond with the GCR particles of $Z \geq 6$ and $LET \geq 1600$ (MeV cm²) g⁻¹ (under the given etching conditions).

The USF stacks were of 3 cm diameter and included CR-39 and Cronar polyester layers. The CR-39 SSNTDs were processed in a 6.25 N NaOH solution for 7 days at 50 °C. The bulk etch, B , was measured for each of the detectors. Pairs of detectors were reassembled in their flight orientations and the two adjacent inner surfaces were scanned with an optical microscope. This procedure permitted the particles to be separated into short-range (SR) (matching tracks appear on two inner surfaces only) and long-range (LR) (matching tracks appear on all four surfaces of the detector pairs) GCR particle tracks. The SR particles include the secondary SR particles from target nuclei within the plastic and the stopping primary GCR and trapped particles. All

‡USF portion of the work partially supported by NASA Grant Nos NCC2-521 (NASA-Ames Research Center) and NAG9-235 (NASA-Johnson Space Center).

protons were detected as SR particles because of their short registration ranges in CR-39. The GCR particles include the primary GCRs and the LR $Z \geq 2$ secondaries which are mainly the GCR projectile fragments. The $Z \geq 2$ stopping GCR particles can also contribute to the SR tracks, but with a low probability.

3. ANALYTICAL PROCEDURE

3.1. Galactic cosmic rays

The GCR particle fluxes outside the Earth's magnetosphere were calculated in terms of the model proposed by Suslov and Nymmik (1988) and described in detail by Suslov and Nymmik (1990). In the model, the energy spectra $F_i(E, t)$ of the $1 \leq Z \leq 28$ GCR particles are inferred from the particle rigidity spectra $\Phi_i(R, t)$:

$$F_i(E, t) dE = \Phi_i(R, t) \frac{A_i \beta}{|z|} dR, \quad (1)$$

where A_i is the atomic number of a nucleus of species i ; R_i is particle rigidity; t is time.

The rigidity spectra are defined by the phenomenological model

$$\Phi_i(R, t) = \frac{D_i \beta^{\alpha_i}}{R_i^{\gamma_i}} \left(\frac{R}{R + R_0(t)} \right)^{\Delta_i(t)}, \quad (2)$$

where D_i , α_i and γ_i are the constants which characterize the spectra of particles of certain species whose values were determined through the available set of experimental data on the GCR particle fluxes during the previous solar cycles.

The data used to calculate the fluxes of all particles can be found in *Standards for Galactic Cosmic Rays* (1991); the constants used in calculating the energy spectra of the basic elements are presented in Table 1. The value of R_0 is defined by the solar activity level and by the delay of the CR particle flux variations relative to Wolf numbers. During the experiment, R_0 proved to be 0.88 GV.

The power-law exponent in (2) is determined by the formula

$$\Delta_i(t) = 5.5 \left[1 + a_i \exp\left(\frac{z_i \beta R}{A_i b_i}\right) \right] + 1.0 \operatorname{sgn}(z_i) \frac{\beta R}{R_0} \exp\left(-\frac{\beta R}{R_0}\right), \quad (3)$$

Table 1. Values of constants used in calculating energy spectra

Element	Z	A_i	D_i	α_i	γ_i
H	1	1	2.0E04	3.0	2.75
He	2	4	3.5E03	3.0	2.75
C	6	12	9.6E01	3.1	2.75
O	8	16	8.4E01	3.0	2.70
Si	14	32	1.2E01	3.0	2.65
Fe	26	56	9.2E00	3.1	2.60

where the coefficients $b_i = 1.2$ and $d_i = 0.034$ describe the form of the spectrum at low energies ($R < 0.55$ GV) and were inferred from our data on the fluence of oxygen nuclei obtained in the Cosmos-2044 experiment (Marenny *et al.*, 1990).

3.2. Function of nuclei penetrating to low orbits

The GCR particle energy spectra on the satellite orbit were found by calculating the penetrating function on the basis of previous determinations of the boundaries for proton penetration into the magnetosphere in a Cosmos-800 experiment (Biryukov *et al.*, 1984).

Figure 1 shows the plots of the penetration function, calculated as indicated above and using the conventional techniques based on the International Reference Geomagnetic Field (IRGF) model. Our approach has yielded higher fluences of particles penetrating to low orbits as compared with conventional techniques (Nymmik, 1991).

3.3. Radiation belt protons

The RB proton fluxes on the Cosmos-2044 orbit were calculated using the AP-8 model (Sawyer and Vetter, 1976) for solar maximum. The calculations have shown that the orbit-integrated differential energy spectrum of the 1–100 MeV protons can be described as

$$F(E) = 8 \times 10^3 E^{-\gamma}, \quad (4)$$

where $\gamma = 2.03$ at $E < 8$ MeV and $\gamma = 2.72$ at $E \geq 8$ MeV.

3.4. Particle flux deep in matter

The species i particle flux under shielding of thickness x is determined by the formula

$$F_x(E'_i) = F_\alpha(L_0/L_x)_i \exp(-x/\lambda_i), \quad (5)$$

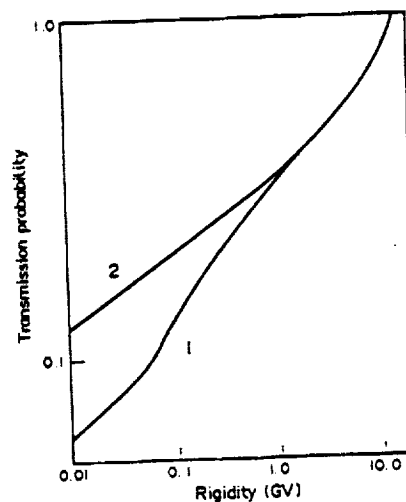


FIG. 1. Particle penetration function into the magnetosphere for the Cosmos-2044 orbit. Curve 1 is the IGRF model calculation result. Curve 2 is the Nymmik (1991) model calculation result.

where $E' = E_0 - \int_0 L_1(x) dx$; L_0 and L_x are the particle LET values above and under the shielding, respectively; λ_i is the species i particle path for nuclear interaction.

The particle energy spectra under the shielding were used to find the particle LET spectra:

$$\Phi_x(>L) = \sum_j \int_L^\infty F_{xy}(E) \left[\frac{dL_i(E)}{dE} \right]^{-1} dL, \quad (6)$$

where $L_i(E)$ is the energy dependence of species i particle LET value; j is a given flux component (GCR or RB).

In conformity with the selection criteria for events in the USF stacks, the flux $\Phi_x(>L)$ was broken into four groups (see Fig. 2):

$$\Phi_x(>L) = \sum_{k=1}^4 \Phi_x^k(>E). \quad (7)$$

If x_1 is the level of the upper surface of the upper detector in a pair of detectors, x_2 is the level of the lower surface of the lower detector in the pair, and x is the level between x_1 and x_2 , then the pictorial pattern for breaking into four groups of events is

κ	1	2	3	4
	GCR	SR ₁	SR ₂	SR ₃
X_1	⊗	○	○	⊗
X	⊗	⊗	⊗	⊗
X_2	⊗	Y	⊗	Y

where ⊗ means that $L > L_0$, ○ means that $L < L_0$, and Y means that a particle is not present. The

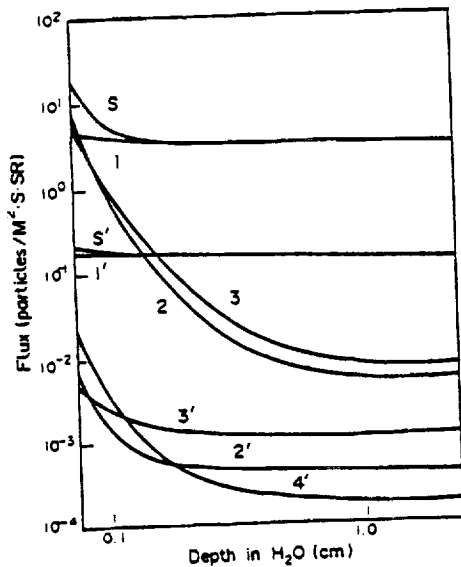


FIG. 2. The calculated flux vs detector depth. Curves 1-4 are particle fluxes calculated by formulas (8)-(11), respectively. S is the total particle flux with $L > L_0$ at depth x . The curves numbered without a prime are for $L > 40 \text{ MeV cm g}^{-1}$; those with a prime are for $L > 1000 \text{ MeV cm g}^{-1}$. Curve 4' is not present for the values of LET and plastic thickness used.

particle fluxes at $L > L_0$ at the level x may be described by

$$\Phi_x^1(\text{GCR}) = \sum_j \Phi_j(L \geq L_0, x_1); (E(R) > E(x_2 - x_1)) \quad (8)$$

$$\Phi_x^2(\text{SR}) = \sum_j \Phi_j(L \geq L_0, x_1); (E(R) \leq E(x_2 - x_1)) \quad (9)$$

$$\Phi_x^3(\text{SR}) = \sum_j \Phi_j(L < L_0, x_1); (E(R) \leq E(x_2 - x_1)) \quad (10)$$

$$\Phi_x^4(\text{SR}) = \sum_j \Phi_j(L < L_0, x_1); (E(R) > E(x_2 - x_1)). \quad (11)$$

In the expressions (8)-(11), the GCR group includes the particles with LET values $L > L_0$ over a range great enough to penetrate both detector layers, from x_1 to x_2 .

4. RESULTS AND DISCUSSION

Figure 2 shows the $\Phi_x^k(L > L_0)$, plots $\Phi_x^1(\text{GCR})$, $\Phi_x^2(\text{SR})$, $\Phi_x^3(\text{SR})$, and $\Phi_x^4(\text{SR})$ calculated for the experimental conditions under the shielding thicknesses ranging from 0.075 to 2.5 cm H_2O at two threshold LET values (40 and 100 $\text{MeV cm}^{-2} \text{g}^{-1}$). From the calculations it follows that, under the shielding exceeding 0.2 cm H_2O , the fraction of the events in groups 2-4 (SR) is less than 1% of all the detected GCR particles, while the events of group 1 include nearly the total fluence of detected CR particles within the given component. Secondary particles are not included in Fig. 2.

Figure 3 shows the experimental data (plotted points) for (a) the particle fluences detected at seven depths at $x > 0.2 \text{ cm H}_2\text{O}$ in the USF stacks (GCR) at $L > 100$ and $L > 500 \text{ MeV cm g}^{-1}$; and (b) at two depths (0.24 and 1.53 cm) in the IMBP stack at $L > 1600 \text{ MeV cm}^2 \text{g}^{-1}$. The independence of the values of GCR particle fluxes predicted by calculations for $L > L_0$ and at depths of 0.1-2.0 g cm^{-2} is confirmed by the data. The measured particle flux at $L > 100 \text{ MeV cm}^2 \text{g}^{-1}$ is somewhat below that predicted by the calculations, but probably within the overall accuracy expected from the comparison.

Figure 3 also presents the data on the events selected by the criteria of SR conditions (9)-(11) and shows the calculated dependence which follows from the RB proton spectrum. This data (Curve 1) has been normalized to the SR particle flux at $x = 0.25 \text{ cm H}_2\text{O}$. To that end, the factor C in (4) had to be set equal to 1000, i.e. eight times less than the value given by the AP-8 model for solar maximum. The reduction in proton flux from the model prediction can be attributed to uncertainties deriving from

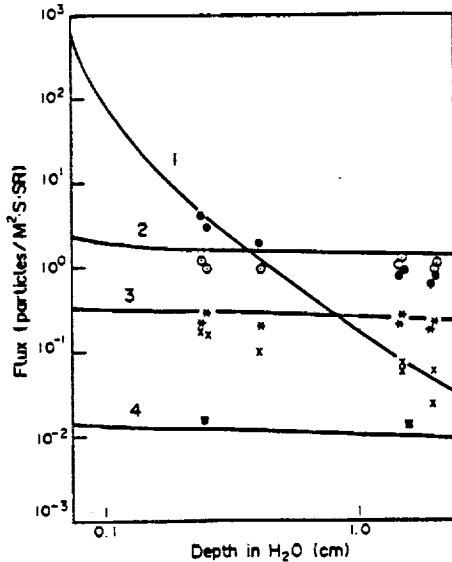


FIG. 3. Particle fluxes with $L > L_c$ vs detector depth. $L > 100 \text{ MeV cm g}^{-1}$: Curve 1 is the SR track density due to RB proton flux calculated by formula (4); Curve 2 is the track density due to GCR particle flux calculated by formulas (1)–(3); the black circles are experimental SR track densities; the circles with dots are experimental GCR track densities. $L > 500 \text{ MeV cm g}^{-1}$: Curve 3 is the track density due to GCR particle flux calculated by formulas (1)–(3); the star-like crosses are experimental GCR track densities; the skewed crosses are the SR track densities. $L > 2 \times 10^3 \text{ MeV cm g}^{-1}$: Curve 4 is the GCR track density calculated by formulas (1)–(3); the squares are the experimental GCR track densities.

two major causes. There are substantial proton flux fluctuations observed at low altitudes near the lower RB border, where the density of residual atmosphere increases. The high solar activity level during the observations may have contributed to atmospheric expansion and a decrease in proton flux. Also, the pronounced directionality of the trapped proton fluxes is not taken into account by the AP-8 model or compensated for by the SSNTDs. The assumption of isotropic proton incidence which is made in correcting the experimental measurements for detector solid angle response could therefore have introduced some error into the measured proton fluxes.

From Fig. 3 it follows that the SR particle flux at $x > 0.3 \text{ cm H}_2\text{O}$ is considerably greater than would be expected from the primary RB protons. For the particle flux with $L > 100 \text{ MeV cm}^2 \text{ g}^{-1}$, the excess equals about 1 particle $(\text{m}^2 \text{ s sr})^{-1}$. Only a small part of this can be attributed to H recoils produced by neutron collisions. The high energy ($> 1 \text{ MeV}$) neutron flux was measured on Cosmos-2044 (Dudkin *et al.*, 1992) in the range of $275\text{--}500 \text{ n}_0/\text{m}^2 \text{ s}^{-1} \text{ sr}^{-1}$. The efficiency of CR-39 for high energy neutron flux detection has been reported as $\sim 10^{-4}$ proton tracks

(neutron) $^{-1}$ (Durrani and Bull, 1987). This would imply a neutron-induced component of ~ 0.04 particles $\text{m}^{-2} \text{ s}^{-1} \text{ sr}^{-1}$. High energy protons also contribute through elastic scattering of target H nuclei and this would seem to be the major source of the excess tracks seen at the larger shielding depths.

The SR particles at $L > 500 \text{ MeV cm}^2 \text{ g}^{-1}$ cannot be protons, but are mainly secondary particles of higher charges produced by inelastic interactions of RB protons and neutrons with the detector nuclei (H, C, O).

REFERENCES

- Benton E. V. and Parnell T. A. (1988) Space radiation dosimetry on US and Soviet manned missions. In *Terrestrial Space Radiation and its Biological Effects*, NATO ASI Series A: Life Sciences, Vol. 154, pp. 729–794. Plenum Press, New York.
- Biryukov A. S., Ivanova T. A., Kovrigin L. M., Kuznetsov S. N., Sosonovets R. N., Tverskaya L. V. and Kudela K. (1984) Boundary of solar cosmic ray penetration into the magnetosphere according to data of Interkosmos-17 and Cosmos-900. *Acta Phys. Slovaca* 34, 153.
- Dudkin V. E., Potapov Yu. V., Akapova A. B., Melkumyan L. V., Rshtuni Sh. B., Benton E. V. and Frank A. L. (1992) Neutron fluences and energy spectra in the Cosmos-2044 biosatellite orbit. *Nucl. Tracks Radiat. Meas.* 20, 139–141.
- Durrani S. A. and Bull R. K. (1987) *Solid State Nuclear Track Detection: Principles, Methods and Applications*, International Series in Natural Philosophy, Vol. 111, Pergamon Press, Oxford.
- Marenny A. M. (1987) *Dielectric Nuclear Track Detectors in Space Radiation and Radiobiology Experiments*. Energoatomizdat, Moscow (in Russian).
- Marenny A. M., Nymmik R. A., Hunyadi I., Csige I., Spurny F., Charvat J. and Guertzen G. R. (1990). Low-energy heavy ions of cosmic rays measured on Cosmos-2044 biosatellite. *Proc. 15th Int. Conf. Particle Tracks Solids*, Marburg, F.R.G., 3–7 September 1990.
- Marenny A. M., Nymmik R. A. and Suslov A. A. (1987) Studies of the fluxes of GCR heavy nuclei using the measurements on board low-orbiting satellites in 1974–1984. *Kosmich. Issled.* 25(4), 577–584.
- Nymmik R. A. (1991) Diurnal variations of geomagnetic cutoff boundary relevant to penetration function. *Kosmich. Issled.* 29(3), 491–493.
- Sawyer D. M. and Vette J. I. (1976) *AP-8 Trapped Proton Environment for Solar Maximum and Solar Minimum*. National Space Science Data Center, Goddard Space Flight Center, NSSDC/WDC-A-R&S 76-06 (June). Also see NASA TM-X-72605 (1976).
- Standards for Galactic Cosmic Rays: Model for Particle Flux Variations* (1991) All-Union State Standard 25645.150-190. Standartizdat, Moscow.
- Suslov A. A. and Nymmik R. A. (1988) Large-scale galactic cosmic ray modulation: energy (rigidity) spectra of protons and He nuclei outside the modulation region. *Izv. Akad. Nauk U.S.S.R., Phys. Ser.* 58(12), 2330–2334.
- Suslov A. A. and Nymmik R. A. (1990) A semi-empirical model for the large-scale modulation of the galactic cosmic ray energy spectra. *Proc. 21st ICRC* 6, 33–37.